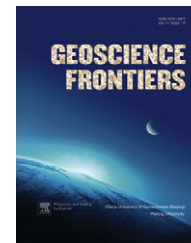


available at [www.sciencedirect.com](http://www.sciencedirect.com)

China University of Geosciences (Beijing)

**GEOSCIENCE FRONTIERS**journal homepage: [www.elsevier.com/locate/gsf](http://www.elsevier.com/locate/gsf)

## RESEARCH PAPER

# Evolution of fracture permeability due to co-colloidal bacterial transport in a coupled fracture-skin-matrix system

N. Natarajan <sup>a,\*</sup>, G. Suresh Kumar <sup>b</sup><sup>a</sup> *EWRE Division, Department of Civil Engineering, Indian Institute of Technology, Madras, Chennai 600036, India*<sup>b</sup> *Department of Ocean Engineering, Indian Institute of Technology, Madras, Chennai 600036, India*

Received 20 August 2011; accepted 1 December 2011

Available online 13 December 2011

**KEYWORDS**

Bacterial transport;  
Colloidal transport;  
Fracture permeability;  
Fracture skin;  
Precipitation-dissolution

**Abstract** A numerical model is developed for investigating the evolution of fracture permeability in a coupled fracture-matrix system in the presence of fracture-skin with simultaneous colloidal and bacterial transport, by taking into account the effects of thermal stress and silica precipitation/dissolution, which is computed using linear reaction kinetics. The non-linear coupled equations are numerically modeled using the fully implicit finite difference method and a constant continuous source is adopted while modeling thermal, contaminant, colloidal and bacterial transport. Due to co-colloid bacterial transport under non-isothermal conditions, in a coupled fracture-skin-matrix system, the fracture apertures vary spatially, with a corresponding pressure variation for a constant discharge. A series of numerical experiments were conducted for analyzing the spatial variation of fracture aperture in response to the combined effects of thermal stress, silica precipitation/dissolution, and simultaneous colloidal and bacterial transport in the presence of the fracture-skin. The simulation results suggest that temperature and contaminant concentration of the mobile fluid within the fracture increases with reduction in initial fracture aperture. The pattern of variation followed by the fracture aperture is nearly the same in the presence and absence of bacterial transport but the magnitude of the fracture aperture is low under the influence of bacterial transport. The variation in the fracture aperture resulting from precipitation-dissolution and

\* Corresponding author.

*E-mail address:* [itsrajan2002@yahoo.co.in](mailto:itsrajan2002@yahoo.co.in) (N. Natarajan).

1674-9871 © 2011, China University of Geosciences (Beijing) and Peking University. Production and hosting by Elsevier B.V. All rights reserved.

Peer-review under responsibility of China University of Geosciences (Beijing).

doi:[10.1016/j.gsf.2011.12.003](https://doi.org/10.1016/j.gsf.2011.12.003)

Production and hosting by Elsevier

thermoelastic stress is significant when the fracture aperture is very low and reduces with increment in fracture aperture. The variation in fracture aperture and pressure remains the same for both undersaturated and supersaturated fluid entering the fracture due to the influence of bacterial transport at the inlet of the fracture.

© 2011, China University of Geosciences (Beijing) and Peking University. Production and hosting by Elsevier B.V. All rights reserved.

## 1. Introduction

Enhanced geothermal reservoir is a major source of renewable energy and the ultimate goal of geothermal reservoir development is to economically develop geothermal energy. One of the important features of the geothermal reservoir is the efficiency of the reservoir which is highly dependent on the permeability through the rock fractures existing within the reservoir. The permeability of fractures is affected by changes resulting from thermal, hydraulic, mechanical, chemical and biological processes. The geothermal fluid interacts with the adjacent rock-matrix leading to the precipitation and dissolution of minerals due to the high gradient in temperature, pressure and concentration between the high permeability fracture and the low permeability rock-matrix. Many studies have been conducted by researchers on precipitation-dissolution in geothermal reservoirs (Robinson, 1982; Robinson and Pendergrass, 1989; Cline et al., 1992; Malate and O'Sullivan, 1992; Lowell et al., 1993; Arvidson and Mackenzie, 1999; Satman et al., 1999; O'Brien et al., 2003; Taron et al., 2009; Taron and Elsworth, 2009). A few studies in the recent past have focused on the aperture and pressure variation resulting from coupled thermal, mechanical and chemical reactions. Suresh Kumar and Ghassemi (2005) developed a numerical model to simulate the combined effect of thermal and reactive solute transport in a coupled fracture-matrix system using dual porosity concepts. The model was applied to examine the mass of silica dissolved/precipitated along the fracture and to compute the change in fracture aperture. Ghassemi and Suresh Kumar (2007) extended the numerical model to include the effect of thermoelastic stress and the temporal variation of the fracture aperture in response to the individual and combined effects of thermal stress and silica dissolution-precipitation was examined. Although most of the studies conducted by the researchers address the evolution of fracture permeability due to coupled processes in a coupled fracture-matrix system, studies dealing with effect of fracture-skin are very few. Fracture-skin is a low permeability material deposited along the fracture walls was pointed out by Sharp (1993). A few studies conducted with respect to solute transport in fracture-skins have concluded that fracture-skins in the form of clay filling (Driese et al., 2001), mineral precipitation (Fu et al., 1993) and organic growth material (Robinson and Sharp, 1997) have reduced the permeability in fracture-skin while some others have concluded that the presence of fracture-skins has increased the permeability in fracture-skins by developing micro-fractures (Polak et al., 2003). The heat and mass transfer mechanisms at the fracture-matrix interface are affected by the presence of fracture-skin. Analogous to solute transport, the presence of fracture-skin can significantly affect the heat conductivity in the fracture-matrix system. Natarajan and Suresh Kumar (2011a) have numerically modeled thermal transport in the coupled fracture-matrix system in the presence of fracture-skin and analyzed the spatial moment of the thermal fronts with the aid of moment

analysis. It was concluded that the presence of fracture-skin can significantly affect the heat transfer mechanism between the fracture and rock-matrix in the geothermal reservoir. Natarajan and Suresh Kumar (2010a) have also analyzed the effect of poroelastic and thermoelastic stresses in the coupled fracture-matrix system in the presence of fracture-skin and have concluded that the effect of poroelasticity is insignificant with respect to fracture aperture for low discharges. Thus, the effect of skin would have a significant impact on the precipitation-dissolution mechanism and thermoelastic stress in the coupled fracture-matrix system. The objective of this work is to study the influence of bacterial transport on the evolution of fracture permeability in a coupled fracture-skin-matrix system subjected to thermal-chemical mechanical processes along with simultaneous colloidal and bacterial transport. Literature review justifies the existence of colloids in a geothermal reservoir (Hurtado et al., 1989; Potapov et al., 2002; Bourcier et al., 2005; McLin et al., 2006). A particular category of bacteria known as thermophilic bacteria which can sustain at very high temperatures in a geothermal reservoir has been reported in the literatures. Yun (1986) has reported the observations on the distribution of thermophilic microorganisms in the hot springs of the volcanic geothermal area of Yunnan province. Sand (2003) has reported the presence of bacteria under aerobic and anoxic conditions in geothermal waters. Significant research has been conducted on colloid facilitated contaminant transport in coupled fracture matrix system (Abdel-Salam and Chrysikopoulos, 1994; Ibraki and Sudicky, 1995; Baek and Pitt, 1996; Chrysikopoulos and Abdel-Salam, 1997; Abdel-Salam and Chrysikopoulos, 1995). As far as transport of colloids in fracture-skin-matrix is concerned, Natarajan and Suresh Kumar (2010b) developed a numerical model for the colloid facilitated radionuclide transport in the coupled fracture-matrix system in the presence of fracture-skin. Their model assumed the radionuclides and colloids to decay as well as sorb on the fracture surface, diffuse into the fracture-skin and the rock-matrix. Filtration as well as remobilization of colloids was also considered in that model and sensitivity analysis was performed to investigate the effect of various colloid properties on the colloid concentration. It was concluded that the presence of colloids hinders the diffusion of contaminants into the rock-matrix. Thus, the presence of colloids and formation of fracture-skin can significantly affect the efficiency of the geothermal reservoir, as they have direct influence on the fracture permeability variation between the injection and production well, resulting from the aperture and pressure variation in the reservoir. Many numerical models have been developed for bacteria facilitated contaminant transport in porous media (Corapcioglu and Haridas, 1984; Corapcioglu and Kim, 1995; Kim and Corapcioglu, 1996; Sen et al., 2005; Kim, 2005, 2006) but very few studies have analyzed the same in the fractured media. Recently Natarajan and Suresh Kumar (2011b) developed a numerical model for bacteria facilitated contaminant transport in a coupled fracture-matrix system. This study is an attempt to study the influence

of bacterial transport in the evolution of fracture permeability and pressure variation due to coupled contaminant, bacteria, colloidal transport along with silica precipitation-dissolution and thermo-elasticity in a coupled fracture-skin-matrix system.

## 2. Physical system and governing equations

The conceptual model corresponding to a coupled fracture-skin-matrix system (Robinson et al., 1998) is illustrated in Fig. 1.

In Fig. 1,  $b$  represents the half fracture aperture,  $d - b$  represents the thickness of the fracture-skin and  $H$  represents the thickness of the half fracture spacing. The following assumptions are used in the present study:

1. The fracture aperture is much smaller in comparison with the length of the fracture;
2. Thermal dispersion is analogous to dispersion of solutes in fracture-matrix system;
3. Convection within the fracture-skin and rock-matrix has been ignored by assuming that there is no fluid flow within the fracture-skin and rock-matrix;
4. Temperature at the fracture-skin interface, i.e., temperature along the fracture walls and along the lower boundary of the fracture-skin is assumed to be equal (at  $y = b$ );
5. Temperature at the skin-matrix interface, i.e., temperature along the upper boundary of the fracture-skin and the lower boundary of the rock-matrix is assumed to be equal (at  $y = d$ ). The conductive flux in the fracture-skin is equal to the conductive flux in the rock-matrix at the skin-matrix interface as expressed in equation;
6. Specific heat capacities are not functions of temperature;
7. The solution is restricted to one-half of the fracture and its adjacent fracture-skin and its associated rock-matrix by assuming symmetry;
8. Thermal conduction is considered both in the fracture, fracture-skin and the rock-matrix;
9. Only a single fluid phase exists;
10. Changes in fluid enthalpy with pressure are neglected;
11. Transverse diffusion and dispersion within the fracture assure complete mixing across the fracture thickness/aperture at all times;
12. Permeability of the fracture-skin and the rock-matrix is low, and molecular diffusion is assumed to be the main transport mechanism in them;
13. Transport along the fracture is much faster than transport in fracture-skin and the rock-matrix;
14. Fracture, fracture-skin and the rock-matrix are saturated;
15. Colloids are assumed to be unaffected by the thermal transport in the fracture and thus precipitation-dissolution is not considered for colloids;
16. Bacteria do not diffuse into the fracture-skin and rock-matrix;
17. The mobile and immobile bacteria cells of a particular strain of bacteria have similar surface characteristics, the

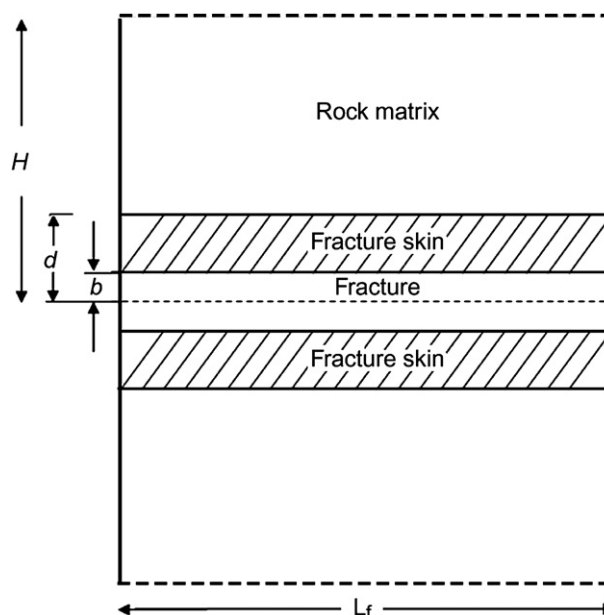


**Figure 1** Schematic diagram showing a coupled fracture-skin-matrix system.

adsorption rate coefficients for both of them are assumed to be same;

18. Sorption of contaminants and bacteria is assumed to follow linear isotherm;
19. Bacteria can survive at high temperatures;
20. The effect of pH is negligible.

The readers are advised to refer Suresh Kumar and Ghassemi (2005) for the governing equations of the flow module. The governing equations and the model assumptions for colloid facilitated contaminant transport have been adopted from Natarajan and Suresh Kumar (2010b) with radioactive decay term to be zero as the contaminants assumed in this model are not radionuclides. The governing equations for thermal transport in fracture-skin-matrix system have been adopted from Natarajan and Suresh Kumar (2011a) to avoid repetition. The governing equations for bacterial facilitated contaminant transport have been adopted from Natarajan and Suresh Kumar (2011b). A pictorial representation of the fractured media involving the contaminants, colloids and bacteria along with the physical processes followed by them has been depicted in Fig. 2.

### 2.1. Bacterial transport in fracture-skin-matrix system

The governing equations for bacteria facilitated contaminant transport in porous media were provided by Corapcioglu and Kim (1995). The equations were modified for fractured media by Natarajan and Suresh Kumar (2011b). The governing equations for contaminant transport are given below.

$$\frac{\partial}{\partial t} \left[ \left( 1 + \frac{K_3 \rho_b}{\theta} + \frac{K_4 K_6 \rho_c \sigma_c}{\theta} + K_5 C_c \right) C_D \right] = D \nabla^2 C_D - \nabla [(1 + K_5 C_c) C_D v] + K_5 D \times \nabla C_c \nabla C_D + K_5 D \times C_D \nabla^2 C_c - \frac{\mu}{Y} \left( C_D + \frac{\rho_b \sigma_D}{\theta} \right) \left( C_c + \frac{\rho_c \sigma_c}{\theta} \right) + \beta k_d \left( C_c + \frac{\rho_c \sigma_c}{\theta} \right) + \frac{\theta_p D_p}{b} \frac{\partial C_{D_s}}{\partial y} \Big|_{y=b} \quad (1)$$

(Natarajan and Suresh Kumar, 2011b)

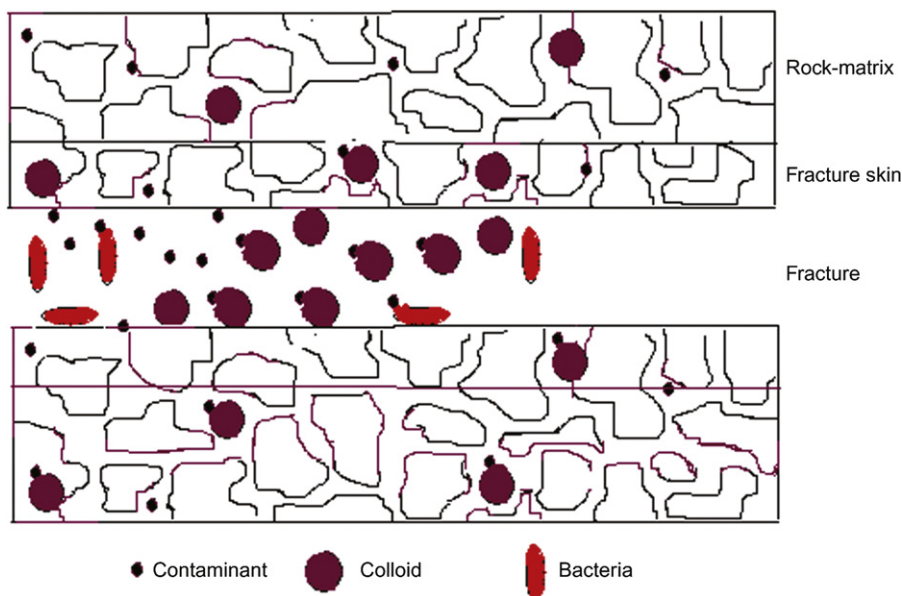


**Figure 2** Pictorial representation of the fractured media along with the colloids, contaminants and bacteria.

where  $K_3$  is the equilibrium distribution coefficient of the dissolved contaminant on the fracture surface,  $\rho_b$  is the bulk density of the fracture-skin,  $\theta$  is the porosity of the fracture-skin,  $K_4$  and  $K_5$  are the equilibrium distribution coefficients for the contaminants with immobile and mobile bacteria,  $K_6$  is the bacterial distribution coefficient between the aqueous phase and the fracture surface,  $\rho_c$  is the density of bacteria,  $\sigma_c$  is the volume fraction of captured bacteria (volume of bacteria captured per unit total volume of the medium),  $C_c$  is the mass concentration of the suspended bacteria in the aqueous phase (mass of bacteria per unit volume of the water phase),  $C_D$  is the mass concentration of contaminant dissolved in the aqueous phase,  $D$  is the hydrodynamic dispersion coefficient,  $v$  is the velocity of the fluid,  $\mu$  is the growth rate of bacteria,  $Y$  is the yield coefficient defined as the mass of microorganisms per unit mass of substrate utilized and is determined from balanced stoichiometric equations,  $\sigma_D$  is the mass fraction of contaminant adsorbed on the fracture surface,  $\beta$  is the conversion factor of dead bacterial cells into contaminant mass (mass of contaminant released per unit mass of dead cells),  $k_d$  is the decay rate coefficient,  $\theta_p$  is the porosity of the fracture-skin,  $D_p$  is the diffusion coefficient of the contaminant in the fracture-skin,  $b$  is the half fracture aperture,  $C_{D_s}$  is the concentration of contaminant in the fracture-skin.

The governing equation for bacterial transport in the fracture:

$$\frac{\partial(\theta R_c C_c)}{\partial t} = D \times \nabla^2(\theta C_c) - v \nabla(\theta C_c) + \mu \theta C_c C_D \cdot \left(1 + \frac{\rho_b K_3}{\theta}\right) \times \left(1 + \frac{\rho_c K_6}{\theta}\right) - k_d \theta C_c \left(1 + \frac{\rho_c K_6}{\theta}\right) \quad (2)$$

(Corapcioglu and Kim, 1995)

where  $R_c$  is the bacterial retardation coefficient expressed as

$$R_c = 1 + \frac{\rho_c K_6}{\theta} \quad (3)$$

The governing equation for contaminant transport in the fracture-skin:

$$\frac{\partial C_{D_s}}{\partial t} = D_p \frac{\partial^2 C_{D_s}}{\partial y^2} \quad (4)$$

The governing equation for contaminant transport in the rock-matrix:

$$\frac{\partial C_{D_m}}{\partial t} = D_m \frac{\partial^2 C_{D_m}}{\partial y^2} \quad (5)$$

where  $D_m$  is the diffusion coefficient of contaminants in the rock-matrix,  $C_{D_m}$  refers to the concentration of the contaminants in the rock-matrix.

The corresponding initial and boundary conditions are given below.

$$C_c(x=0, t) = C_{c_0} \quad (6)$$

$$C_c(x=L, t) = 0 \quad (7)$$

$$C_c(x, t=0) = C_D(x, t=0) = C_{D_m}(x, y, t=0) = C_{D_s}(x, y, t=0) = 0 \quad (8)$$

$$C_D(x=L, t) = 0 \quad (9)$$

$$C_D(x=0, t) = C_{D_0} \quad (10)$$

$$C_{D_s}(x, y=b, t) = C_D(x, t) \quad (11)$$

$$C_{D_s}(x, y=d, t) = C_{D_m}(x, y=d, t) \quad (12)$$

$$\theta_p D_p \frac{\partial C_{D_s}(x, y=d, t)}{\partial x} = \theta_m D_m \frac{\partial C_{D_m}(x, y=d, t)}{\partial x} \quad (13)$$

$$\frac{\partial C_{D_m}(x, y=H, t)}{\partial y} = 0 \quad (14)$$

### 2.2. Precipitation-dissolution of quartz in the fracture-skin-matrix system

The principal solute transport mechanisms in the fracture are advection, describing the motion of dissolved particles along the circulating fluid, free molecular diffusion within the fracture in the direction of fracture axis, diffusion limited solute transport at the fracture-skin interface, dissolution of quartz within the fracture and effective diffusion within the fracture-skin. The coupling between the fracture and skin is ensured by the continuity of the fluxes between them by assuming that the conductive flux from the fracture to the skin takes place in a direction perpendicular to the fracture. The quartz dissolution is described by linear reaction kinetics and the modified form of fracture, fracture-skin and matrix equations are given by Steefel and Lichtner (1998):

$$\frac{\partial S}{\partial t} = v_f \frac{\partial S}{\partial x^2} - k_f S + \frac{\theta_p D_p}{b} \frac{\partial S_p}{\partial y} \Big|_{y=b} \quad (15)$$

$$\frac{\partial S_p}{\partial t} = D_p \frac{\partial^2 S_p}{\partial y^2} - \frac{k_p}{\theta_p} S_p \quad (16)$$

$$\frac{\partial S_{mat}}{\partial t} = D_{mat} \frac{\partial^2 S_{mat}}{\partial y^2} - \frac{k_{mat}}{\theta_{mat}} S_{mat} \quad (17)$$

where  $k$ ,  $k_p$ ,  $k_{mat}$  refer to the rate constant in the fracture, fracture-skin and in the rock-matrix, which are dependent on temperature. The quartz concentration in the fracture, fracture-skin and rock-matrix can be obtained using the expressions given below:

$$S = S - S^{eq} \quad (18)$$

$$S_p = S_p - S_p^{eq} \quad (19)$$

$$S_{mat} = S_{mat} - S_{mat}^{eq} \quad (20)$$

where  $S$  is the total dissolved concentration in the fracture,  $S_p$  is the total dissolved concentration in the fracture-skin and  $S_{mat}$  is the total dissolved concentration in the rock-matrix.  $S^{eq}$ ,  $S_p^{eq}$  and  $S_{mat}^{eq}$  are the equilibrium concentration in fracture, fracture-skin and matrix which are temperature dependent.

The initial and boundary conditions associated with equations (4)–(6) are as follows:

$$S(x, t=0) = S_p(x, y, t=0) = S_{mat}(x, y, t=0) = 0 \quad (21)$$

$$S(x=0, t) = S_0 \quad (22)$$

$$S(x=L_f, t) = 0 \quad (23)$$

$$S(x, t) = S_p(x, y=b, t) \quad (24)$$

$$\theta_p D_p \frac{\partial S_p(x, y=d, t)}{\partial y} = \theta_{mat} D_{mat} \frac{\partial S_{mat}(x, y=d, t)}{\partial y} \quad (25)$$

$$S_p(x, y=d, t) = S_{mat}(x, y=d, t) \quad (26)$$

$$\frac{\partial S_{mat}(x, y=H, t)}{\partial y} = 0 \quad (27)$$

The temperature dependent equilibrium concentration adopted by Robinson and Pendergrass (1989) from Rimstidt and Barnes (1980) is

$$S^{eq} = 6 \times 10^4 \times 10^{(1.881 - 2.028 \times 10^{-3} T - 1560/T)} \quad (28)$$

where equilibrium concentration is in ppm and temperature is in K.

The temperature dependent dissolution rate constant is given by Robinson (1982)

$$k = 10^{(0.433 - 4090/T)} \quad (29)$$

where the units of  $k$  are m/s.

In order to compute the mass of silica deposited along in the fracture at various times, the cumulative mass of silica dissolved along the fracture is examined using the approach followed by Robinson and Pendergrass (1989). For each time interval, the mass of silica dissolved per unit fracture length is given by

$$m_q = \frac{10^{-6} \rho_w \Delta t V_f k a^* (S^{eq} - S)}{L_f} \quad (30)$$

where  $\rho_w$  is the density of the circulating fluid in the fracture,  $V_f (= A_f \times L_f)$  is the volume of fluid in the fracture,  $L_f$  is the length of the fracture and  $A_f (= 2b \times 1)$  is the cross-sectional area of the fracture perpendicular to the flow direction. Since the fluid flow occurs in the fractures, a relationship is developed for  $a^*$  assuming that the fracture can be approximated by the parallel plate model:

$$a^* = \frac{2f_q}{2b} \quad (31)$$

where  $f_q$  is the volume fraction of quartz in the rock-matrix and  $2b$  is the mean fracture aperture. The quantity of silica dissolved in the fracture is related to the fractional aperture change in the average fracture aperture by assuming the fracture flow geometry (Robinson and Pendergrass, 1989). For each time step, the fractional aperture change,  $\Delta w$ , resulting from the chemical interaction between the fracture and rock-matrix is related to the function of total rock-matrix volume and its components and is given as (Robinson and Pendergrass, 1989).

$$\Delta w = \frac{-L_f m_q}{\rho_q V_f} \quad (32)$$

where  $\rho_q$  is the density of quartz,  $V_f$  is the fluid volume in the fracture,  $L_f$  is the length of the fracture.

### 2.3. Fracture aperture change due to thermoelasticity

The expression for rock displacement as a function of temperature is given by Ghassemi and Suresh Kumar (2007) has been modified.

$$\frac{\partial u_y}{\partial t} = \frac{1}{2} \frac{\partial w(x, t)}{\partial t} = \frac{(1 + \nu) \alpha_T \lambda_s}{(1 - \nu) \rho_s C_s} \frac{\partial \Delta T(x, y, t)}{\partial y} \Big|_{y=0} \quad (33)$$

where  $\nu$  is the Poisson's ratio and  $\alpha_T$  is the linear thermal expansion coefficient.

The analytical solution for heat flux at the interface of the fracture and rock-matrix given by Bodvarsson (1969) has been modified to account for the fracture-skin.

$$\frac{T_{s0} - T(x, y, t)}{T_{s0} - T_{f0}} = \operatorname{erfc} \left[ \frac{\sqrt{\lambda_s \rho_s C_s}}{QC_w \rho_w \sqrt{t}} x + \sqrt{\frac{\rho_s C_s}{\lambda_s t}} \frac{y}{2} \right] \quad (34)$$

where  $T_{s0}$  is the initial fracture-skin temperature,  $T_{f0}$  is the initial injection fluid temperature,  $Q$  the volumetric injection rate,  $\rho_w$  the fluid density and  $C_w$  is the water specific heat. If we assume the temperature at infinity is  $T_{s0}$  and  $\Delta T = T_{s0} - T_{f0}$ , we can write equation (20) as:

$$T(x, y, t) - T_{s0} = -\Delta T \operatorname{erfc} \left[ \frac{x\sqrt{\lambda_s \rho_s C_s}}{QC_w \rho_w \sqrt{t}} + \sqrt{\frac{\rho_s C_s}{\lambda_s t}} \frac{y}{2} \right] \quad \text{or}$$

$$T(x, y, t) - T_{s0} = -\Delta T \operatorname{erfc}(A_1 + A_2 y)$$

$$\text{where } A_1 = \frac{x\sqrt{\lambda_s \rho_s C_s}}{QC_w \rho_w \sqrt{t}} \text{ and } A_2 = \sqrt{\frac{\rho_s C_s}{\lambda_s t}} \frac{1}{2}$$

Differentiating equation (20) with respect to  $y$ :

$$\begin{aligned} \left. \frac{\partial \Delta T(x, y, t)}{\partial y} \right|_{y=0} &= \frac{2\Delta T A_2}{\sqrt{\pi}} \exp[-(A_1 + A_2 y)^2] \\ &= \frac{2\Delta T A_2}{\sqrt{\pi}} \exp[-(A_1)^2] \end{aligned} \quad (35)$$

Substituting equation (21) into equation (19) yields:

$$\frac{\partial w(x, t)}{\partial t} = \frac{2(1+\nu)\alpha_T \lambda_s}{(1-\nu)\rho_s C_s} \left( \frac{2\Delta T A_2}{\sqrt{\pi}} \exp[-(A_1)^2] \right) \quad (36)$$

### 3. Numerical model

In this study, the system is described by a set of three partial differential equations, one equation for the fracture, one for the fracture-skin and the remaining for the rock-matrix, formulated for a one-dimensional framework. The system of equations is non-linear and couples the fracture, fracture-skin and the rock-matrix. The coupled system is solved numerically using implicit finite difference scheme. The continuity at the fracture-skin interface is attained by iterating the solution at each time step. This is carried out in solving contaminant transport facilitated by colloids and bacteria, thermal transport, and reactive transport. A non-uniform grid is adopted in the fracture-skin and rock-matrix. A smaller grid size is adopted in the fracture-skin interface to accurately capture the flux transfer at the fracture-skin interface.

Initially, the contaminant concentration facilitated by colloids and bacteria is obtained by solving the governing equations pertaining to colloid facilitated contaminant transport from Natarajan and Suresh Kumar (2010b) and bacteria facilitated contaminant transport in a coupled fracture-skin-matrix system from Natarajan and Suresh Kumar (2011a,b). The temperature distribution along the fracture in the coupled system is obtained by solving the governing equations for thermal transport in the domain. Having found the temperature distribution, the thermoelastic changes in fracture aperture are calculated using the analytical solution provided in equation (36) and the new fracture aperture is computed. The computed temperature distribution is then used to calculate the reaction constants for the fracture, fracture-skin and the rock-matrix using equation (29) and thus evaluate the new equilibrium concentration of silica using equation (28). The reaction constants along with the existing contaminant concentration are used to calculate the total dissolved concentration using

equations (15)–(17). This concentration is finally used in computing the quartz concentration in the fracture, fracture-skin and rock-matrix using equations (18)–(20). Based on this quartz concentration, the mass of silica deposited/dissolved is computed using equation (30) and the aperture change is calculated using expression (32). The new fracture aperture is obtained by adding this with the previous value. The final updated fracture aperture is used to calculate the pressure variation using the Cubic law. The old values of temperature and concentration profiles are updated for the next time step. An iteration process is carried out as shown below between the fracture and fracture-skin temperatures and concentrations at the fracture and skin interface. The coupling between the various components described above has been shown using a flow chart in Fig. 3.

The discretization of the coupling term representing the last term in equation (15) indicates the coupling at the interface of the fracture and the fracture-skin. This coupling is discretised as

$$\frac{\partial S_p}{\partial t} = \frac{S_{p2}^{n+1} - S_{p1}^{n+1}}{\Delta y(1)}$$

The concentration in the first node of the fracture-skin becomes equal to the fracture concentration at the interface of the fracture and the fracture-skin satisfying the assumed boundary condition, i.e.,

$$S_{p1}^{n+1} = S^{n+1}$$

Since the concentration of the second node in the fracture-skin ( $S_{p2}^{n+1}$ ) is known only at the initial time ( $t = 0$ ) and is unknown at the next time step, i.e.,  $(n+1)^{\text{th}}$ , the value is assumed and iterated until convergence is achieved. Thus the concentrations for the  $i^{\text{th}}$ ,  $(i-1)^{\text{th}}$  and  $(i+1)^{\text{th}}$  nodes are solved at the next time step, i.e.,  $(n+1)^{\text{th}}$  and the fourth unknown in the equation ( $S_{p2}^{n+1}$ ) is assumed and iterated until convergence is achieved.

### 4. Results and discussion

An implicit finite difference numerical model is developed to determine the evolution of fracture permeability and fluid pressure resulting from precipitation-dissolution of quartz in the presence of fracture-skin and contaminant transport facilitated by colloids and bacteria. The study considers situations in which the water entering the fracture, either supersaturated or undersaturated with respect to quartz flows through the fracture-skin-matrix system. As the water entering the fracture gets heated by conduction, cools the rock, leading to thermal stress in the rock mass and changes the silica concentration in the fracture.

A scaled/relative concentration can be any concentration that is conserved in a chemical reaction (Ghassemi and Suresh Kumar, 2007). The equilibrium concentration obtained from Rimstidt and Barnes (1980), in terms of parts per million, is converted into mmol/L by dividing by the molecular weight of silica (60.08 g/mol). Depending on the nature of the injected fluid, the contaminant concentration at the inlet of the fracture (or injection well) may be maintained either at undersaturated or oversaturated concentration. A scaled/relative concentration of 1.0 is used as the boundary condition at the injection well, so that the constant relative contaminant concentration at the fracture inlet could be 0.25 (25 mmol/L) or 0.02 (2 mmol/L) when the injection fluid is oversaturated or undersaturated with

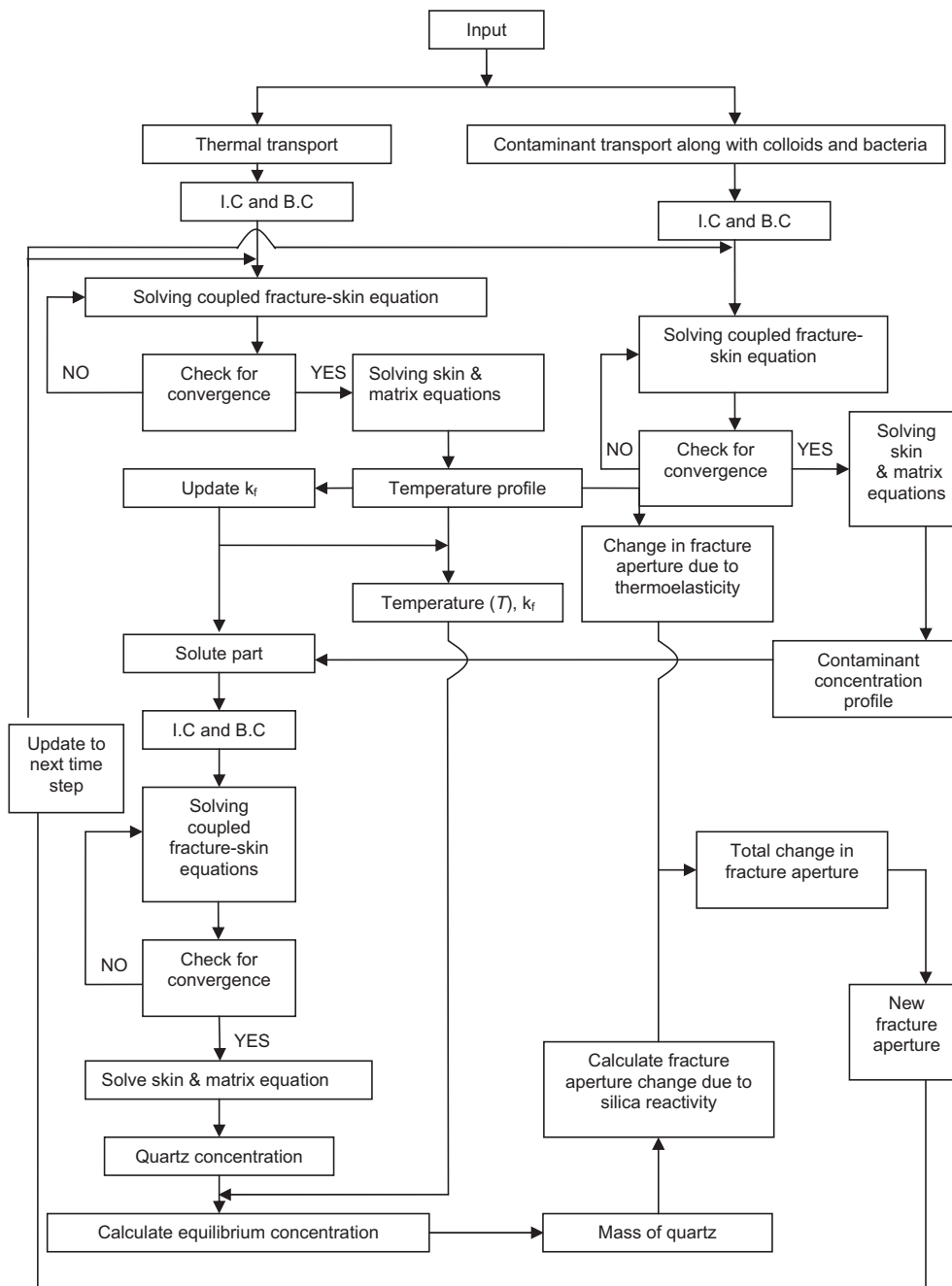


**Figure 3** Coupling of contaminant transport, heat transport and reactive solute transport in a coupled fracture-skin-matrix system.

respect to quartz, respectively (Ghassemi and Suresh Kumar, 2007). The equilibrium concentration value for quartz is 10 mmol/L.

The dataset that was adopted by Natarajan and Suresh Kumar (2010b) in simulating colloid facilitated contaminant transport in fracture-skin-matrix system has been adopted for this study also. The parameters are provided in Table 1. The dataset used for thermal transport in fracture-skin-matrix system is given in Table 2.

The dataset that was adopted by Natarajan and Suresh Kumar (2011a,b) in simulating bacteria facilitated contaminant transport in fracture-skin-matrix system has been adopted for this study also. The parameters are provided in Table 3.

In this section, the aperture and pressure variation along the fracture are analyzed for the combined effects of chemical, thermal and biological effects.

Fig. 4 shows the comparison of fracture aperture variation for various initial half fracture apertures under the combined effects of thermoelastic stress and chemical effects, in the presence and absence of bacterial transport. It is observed from Fig. 4 that the pattern of variation followed by the fracture aperture is nearly the same in the presence and absence of bacterial transport but the magnitude of the fracture aperture is low when bacterial transport is considered. As in all the above cases, the variation of fracture aperture is very low in the presence of bacterial growth, proliferation of bacteria in small fracture apertures would decrease the

**Table 1** Parameters used for the colloid facilitated contaminant transport.

Parameter	Symbol	Value
Initial half fracture aperture (m)	$b$	$200 \times 10^{-6}$
Fracture-skin thickness (m)	$d - b$	0.02
Fracture spacing (m)	$2H$	0.2
Diffusion coefficient of contaminants within the fracture-skin ( $m^2/y$ )	$D_P$	0.01
Diffusion coefficient of contaminants within the rock-matrix ( $m^2/y$ )	$D_{mat}$	0.01
Porosity of the fracture-skin		0.09
Distribution coefficient for contaminants on the fracture surface (m)	$K_{ds}$	0
Distribution coefficient for contaminants in fracture-skin (m)	$K_{dsP}$	0
Distribution coefficient for contaminants in rock-matrix (m)	$K_{dsmat}$	0
Hydrodynamic dispersion coefficient of contaminants dissolved in the fracture aqueous phase ( $m^2/y$ )	$D$	10
Distribution coefficient for contaminants with mobile colloids within the fracture (for colloid diameter of 300 nm) ( $m^3/kg$ )	$K_{dm}$	40
Distribution coefficient for contaminants with immobile colloids within the fracture ( $m^3/kg$ )	$K_{dim}$	40
Distribution coefficient for contaminants with mobile colloids within the fracture-skin ( $m^3/kg$ )	$K_{dmP}$	40
Distribution coefficient for contaminants with immobile colloids within the fracture-skin ( $m^3/kg$ )	$K_{dimP}$	40
Distribution coefficient for contaminants with mobile colloids within the rock-matrix ( $m^3/kg$ )	$K_{dmmat}$	40
Distribution coefficient for contaminants with immobile colloids within the rock-matrix ( $m^3/kg$ )	$K_{dimmat}$	40
Average velocity of colloids in the fracture (m/y)	$V_C$	1
Colloid concentration at the inlet of the fracture ( $kg/m^3$ )	$C_o$	1
Hydrodynamic dispersion coefficient of colloids suspended in the rock fracture ( $m^2/y$ )	$D_C$	1
Filtration coefficient for colloids ( $m^{-1}$ )	$\lambda_f$	0.5
Percentage of diffusion for colloids	$\varepsilon$	0.5
Diffusion coefficient of colloids within the fracture-skin ( $m^2/y$ )	$D_{CP}$	$2.2 \times 10^{-8}$
Diffusion coefficient of colloids within the rock-matrix ( $m^2/y$ )	$D_{Cmat}$	$1.5 \times 10^{-9}$
Distribution coefficient for colloids within the fracture-skin	$K_{dCP}$	0.1
Distribution coefficient for colloids within the rock-matrix	$K_{dCmat}$	0.01
Remobilization coefficient for colloids in the fracture ( $y^{-1}$ )	$Rmb$	0.5
Length of the fracture (m)	$L$	50
Total simulation time (y)	$t$	5
Concentration of contaminants at the inlet of the fracture ( $kg/m^3$ )	$N_0$	1

reservoir efficiency significantly since the flow rate would reduce drastically with decrement in fracture aperture. It has to be noted that flow in a fracture is based on Cubic law where discharge is directly proportional to cube of the fracture aperture. Therefore, even a minor variation in the fracture aperture would affect the discharge in the fracture and consequently would affect the reservoir efficiency as it is directly dependent on the fracture permeability. The fracture aperture is the same at the inlet of the fracture with and without bacterial transport for different initial fracture apertures but varies away from the fracture inlet. The reduction in the magnitude of the fracture aperture when subjected to bacterial transport is due to the consumption of contaminants by bacteria as substrate. This reduces the contaminant concentration nearer to the inlet of the fracture and thus affects the precipitation-dissolution of silica along the fracture. It is observed from Fig. 4 that for high fracture apertures, the magnitude difference in the fracture aperture with and without the consideration of bacterial transport is minimal and this difference increases with the reduction in the fracture aperture. When the fracture aperture is very low ( $b = 1 \times 10^{-6}$  m), the magnitude difference is very high, specifically toward the farther end of the fracture.

Fig. 5 shows the comparison of pressure variation for various initial half fracture apertures under the combined effects of thermoelastic stress and chemical effects, in the presence and absence

of bacterial transport. It is observed from Fig. 5 that the pattern of variation followed by the pressure distribution is nearly the same in the presence and absence of bacterial transport but the magnitude of pressure distribution is high when bacterial transport is considered. Fig. 5 shows the variation in pressure along the fracture corresponding to the aperture variation shown in the previous figure. The pressure variation is low for very high initial fracture apertures and the variation increases with reduction in initial fracture aperture. Similar to the fracture aperture variation, it is observed from Fig. 5 that for high fracture apertures, the magnitude difference in pressure with and without the consideration of bacterial transport is minimal and the difference increases with the reduction in the fracture aperture. Pressure variation is observed throughout the length of the fracture for very small fractures compared to large fractures. Thus, the growth of bacteria is a case of concern for small fractures rather than large fractures. Bacterial growth can significantly affect the geothermal reservoirs consisting of very small fracture aperture thickness and thereby affect the reservoir efficiency.

Fig. 6 shows the comparison of temperature variation for various initial half fracture apertures, in the presence and absence of bacterial transport. It is observed from Fig. 6 that the temperature variation along the fracture is the same with and without the consideration of bacterial transport. This is because bacterial transport does not influence the thermal transport in the fracture

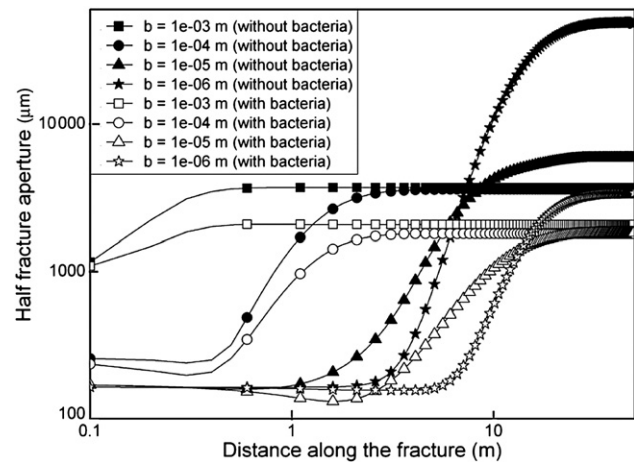
**Table 2** Parameters used for thermal transport in fracture-skin-matrix system.

Parameter	Symbol	Value
Initial fracture aperture (μm)	<i>b</i>	200
Thermal dispersivity (m)	$\beta_T$	0.05
Rock-matrix specific heat capacity (J/kg/K)	$C_m$	800
Rock density (kg/m <sup>3</sup> )	$\rho_m$	2600
Thermal conductivity of the rock-matrix (W/m-K)	$\lambda_m$	2
Specific heat capacity of the fracture-skin (J/kg/K)	$C_s$	1500
Fracture-skin density (kg/m <sup>3</sup> )	$\rho_s$	1500
Thermal conductivity of the fracture-skin (W/m-K)	$\lambda_s$	2
Rock-matrix porosity	$\theta$	0.05
Specific heat capacity of fracture fluid (J/kg/K)	$C_f$	5000
Fracture fluid density (kg/m <sup>3</sup> )	$\rho_f$	1000
Thermal conductivity of fracture fluid (W/m-K)	$\lambda_f$	0.5
Initial temperature (matrix and fracture) (K)	$T_0$	600
Temperature at the inlet of the fracture (K)	$T_i$	300
Length of the fracture (m)	$L$	50
Total simulation time (y)	$T$	5
Poisson's ratio	$\nu$	0.25
Linear thermal expansion coefficient (K <sup>-1</sup> )	$\alpha_T$	$8 \times 10^{-6}$
Volume fraction of quartz in rock-matrix		0.2

and it has also been assumed that the bacterial transport is not affected by the high temperature within the fracture. From Fig. 6, it can be observed that as the half fracture aperture is reduced, the relative temperature in the fracture takes a longer time to attain the rock-matrix temperature. This is because, as the fracture aperture is reduced, the velocity of the fluid increases. This reduces the residence time for the fluid to extract heat from the fracture-skin and thus matrix temperature is attained far away from the fracture inlet even in the presence of fracture-skin.

**Table 3** Parameters used for bacteria facilitated contaminant transport.

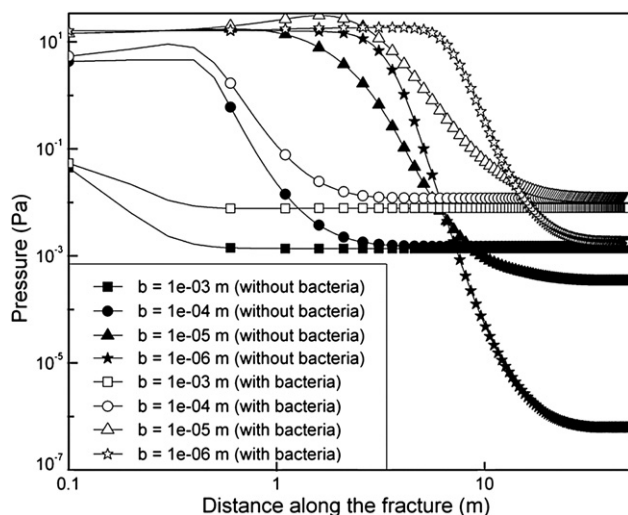
Parameter	Symbol	Value
Initial fracture aperture (μm)	<i>b</i>	200
Fluid velocity (m/y)	<i>V</i>	1
Density of bacteria (kg/m <sup>3</sup> )	$\rho_c$	1700
Length of the fracture (m)	$L_f$	50
Specific growth rate (1/y)	$\mu$	1.5
Monod's half saturation constant ( $K_s$ )	kg/m <sup>3</sup>	0.1
Bacteria decay rate (1/y)	$k_d$	$10 \times 10^{-3}$
Yield coefficient	<i>Y</i>	0.1
Concentration of bacteria at the inlet of the fracture (kg/m <sup>3</sup> )	$C_{C_0}$	0.01
Equilibrium distribution coefficient of the dissolved contaminant on the fracture surface (m <sup>3</sup> /kg)	$K_3$	0.01
Equilibrium distribution coefficient of the contaminant on the mobile and immobile bacteria (m <sup>3</sup> /kg)	$K_4, K_5$	10
Equilibrium distribution coefficient of the bacteria in the aqueous phase and the fracture surface (m <sup>3</sup> /kg)	$K_6$	0.1
Total simulation time (y)	<i>t</i>	5



**Figure 4** Comparison of variation of half fracture aperture along the fracture for various initial half fracture apertures under the combined effects of thermoelastic stress and chemical effects, along with and without the influence of bacterial transport ( $t = 5$  yrs, Flow rate =  $5 \times 10^{-4}$  m<sup>3</sup>/y, fluid entering the fracture is undersaturated (300 ppm), Refer Tables 1–3 for other data).

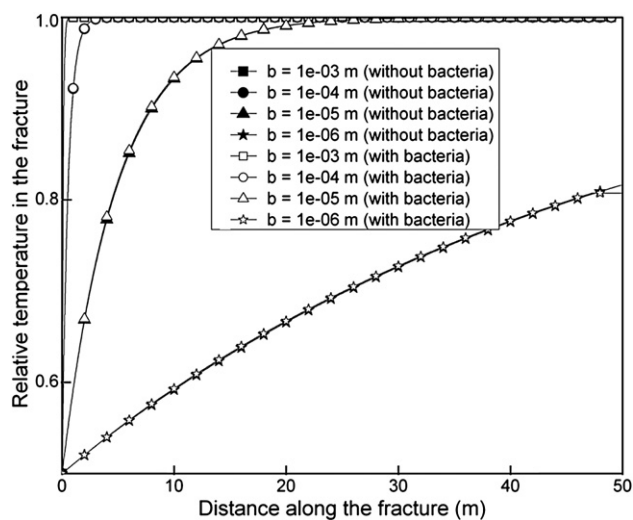
Fig. 7 shows the spatial distribution of contaminant concentration for various initial half fracture apertures due to combined thermoelastic stress, chemical and biological effects. It is observed from Fig. 7 that the concentration of contaminants increases in the fracture with reduction in half fracture aperture, unlike the usual observation where the contaminant concentration in the fracture reduces with reduction in fracture aperture due to significant matrix diffusion. This is because of the filtration of colloids from the aqueous phase, which increases with reduction in fracture aperture. This reduces the diffusion of colloids and contaminants into the fracture-skin. Therefore, colloid transport mechanism differs from the solute transport process in fractures. Moreover, the influence of colloidal transport mechanism on contaminant transport would affect the fracture permeability for various half fracture apertures and thereby affect the reservoir efficiency.

Fig. 8 shows the change in the fracture aperture is due to chemical precipitation for various initial half fracture apertures. It is observed from Fig. 8 that the variation in the fracture aperture



**Figure 5** Comparison of variation of pressure along the fracture for various initial half fracture apertures under the combined effects of thermoelastic stress and chemical effects, along with and without the influence of bacterial transport ( $t = 5$  yrs, Flow rate =  $5 \times 10^{-4}$  m<sup>3</sup>/y, fluid entering the fracture is undersaturated (300 ppm), Refer Tables 1–3 for other data).

resulting from precipitation-dissolution is significant when the fracture aperture is very low and is observed throughout the length of the fracture. This is because the temperature variation gradually occurs along the fracture for low fracture apertures (as observed in Fig. 6) which aids in precipitation-dissolution to occur throughout the domain. For initial fracture aperture of  $1 \times 10^{-4}$  m, the fracture aperture variation occurs within 5 m from the fracture inlet and remains constant thereafter. For large fracture aperture of  $1 \times 10^{-3}$  m, the aperture variation is very low and occurs very near to the fracture inlet compared. This is because as the fracture



**Figure 6** Comparison of spatial distribution of relative temperature along the fracture for various initial half fracture apertures with and without the influence of bacteria, Flow rate =  $5 \times 10^{-4}$  m<sup>3</sup>/y. Fluid entering the fracture is undersaturated (300 ppm). Refer Tables 1–3 for other data.

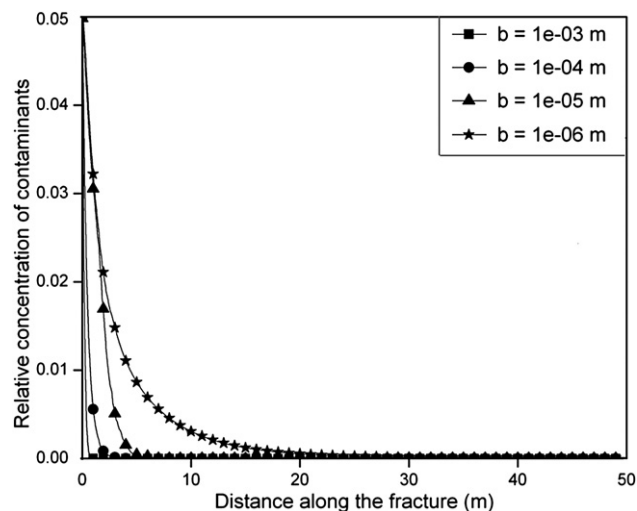


**Figure 7** Spatial distribution of contaminant concentration along the fracture for various initial half fracture apertures, Flow rate =  $5 \times 10^{-4}$  m<sup>3</sup>/y. Fluid entering the fracture is undersaturated (300 ppm). Refer Tables 1–3 for other data.

aperture becomes larger, the coupling between the fracture and the adjacent rock-matrix with fracture skin reduces. In addition, heat diffusion takes place rapidly (as observed in Fig. 6), resulting in minor aperture variation.

Fig. 9 shows the change in the fracture aperture due to thermoelastic stress for various initial half fracture apertures. It is observed from Fig. 9 that the variation in the fracture aperture resulting from thermoelastic stress is significant when the fracture aperture is very low and is observed throughout the length of the fracture. This is because for low initial fracture apertures, thermal transport occurs throughout the length of the fracture due to high fluid velocity which provides low residence time for heat diffusion.

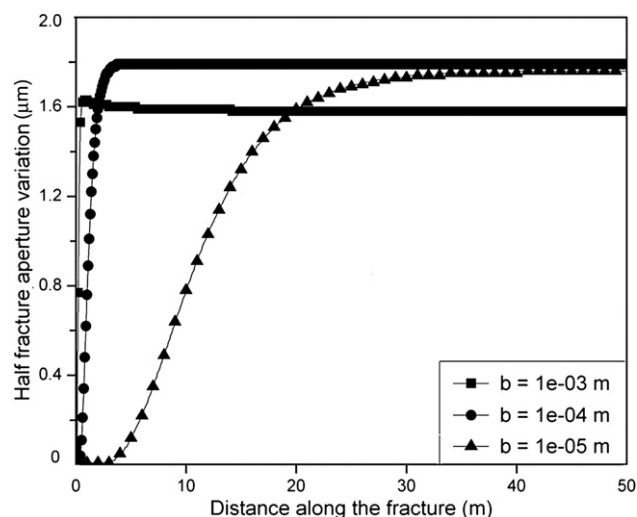


**Figure 8** Change in half fracture aperture due to chemical precipitation for various initial half fracture apertures, Flow rate =  $5 \times 10^{-4}$  m<sup>3</sup>/y. Fluid entering the fracture is undersaturated (300 ppm). Refer Tables 1–3 for other data.

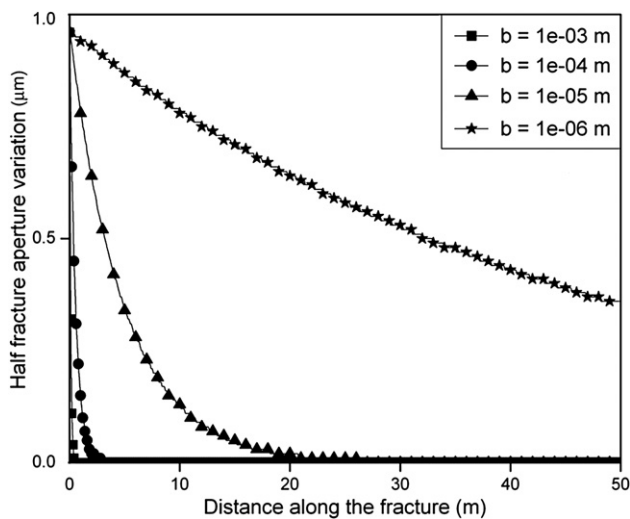
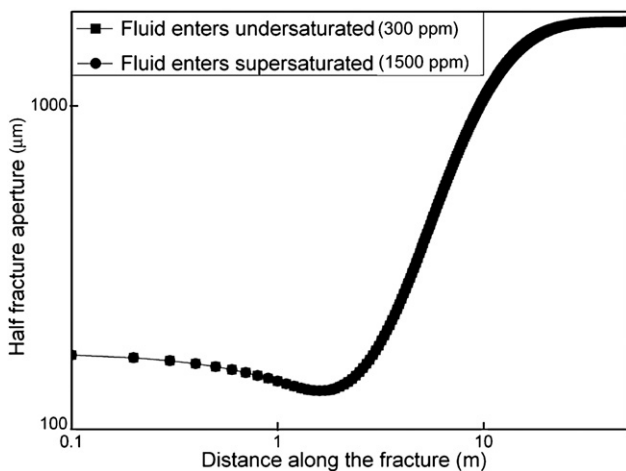


**Figure 9** Change in half fracture aperture due to thermoelastic stress for various initial half fracture apertures, Flow rate =  $5 \times 10^{-4} \text{ m}^3/\text{y}$ . Fluid entering the fracture is undersaturated (300 ppm). Refer Tables 1–3 for other data.

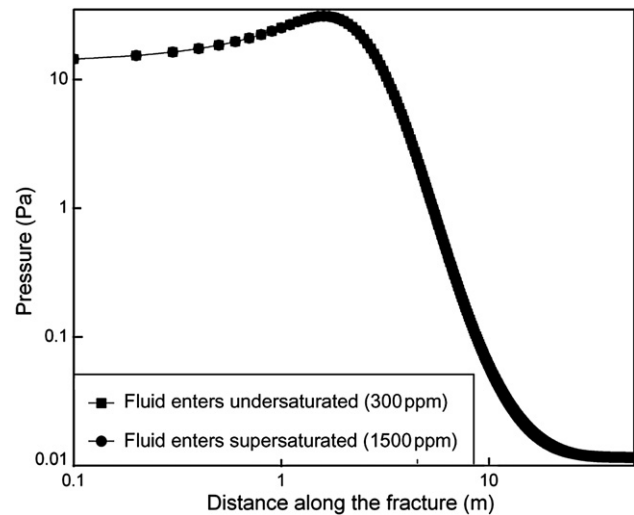
For low initial fracture apertures of  $1 \times 10^{-4} \text{ m}$  and  $1 \times 10^{-3} \text{ m}$ , the fracture aperture variation occurs within 5 m from the fracture inlet due to instantaneous heat transfer between the fracture and the fracture-skin.

Fig. 10 shows the variation in the half fracture aperture when undersaturated and supersaturated fluid enters the fracture. A constant flow rate of  $5 \times 10^{-4} \text{ m}^3/\text{y}$  has been assumed. It is observed that the aperture variation remains the same for both undersaturated and supersaturated cases. This is because of the influence of bacterial transport at the inlet of the fracture.

Fig. 11 shows the variation in pressure when undersaturated and supersaturated fluid enters the fracture. A constant flow rate of  $5 \times 10^{-4} \text{ m}^3/\text{y}$  has been assumed. It is observed that the pressure variation corresponding to the aperture variation remains the same for both undersaturated and supersaturated cases.



**Figure 10** Variation in half fracture aperture along the fracture when undersaturated and supersaturated fluid is entering into the fracture ( $t = 5 \text{ yrs}$ , initial fracture aperture  $b_0 = 1 \times 10^{-5} \text{ m}$ , Flow rate =  $5 \times 10^{-4} \text{ m}^3/\text{y}$ ). Refer Tables 1–3 for other data.



**Figure 11** Variation in pressure along the fracture when under and supersaturated fluid is entering into the fracture ( $t = 5 \text{ yrs}$ , initial fracture aperture  $b_0 = 1 \times 10^{-5} \text{ m}$ , Flow rate =  $5 \times 10^{-4} \text{ m}^3/\text{y}$ ). Refer Tables 1–3 for other data.

### 5. Conclusion

A numerical model has been developed to investigate the influence of simultaneous colloidal and bacterial transport on the evolution of fracture permeability due to the heat induced thermoelastic stress and silica water interaction in the coupled fracture-skin-matrix system. Mass exchange between the horizontal fracture and the fracture-skin is accounted for by assuming diffusion limited transport for both colloids as well as contaminants. The heat transfer between the fracture and the fracture-skin was modeled using the lateral conduction heat flux from the fracture-skin to the fracture, while the heat transport in the fracture was modeled by considering thermal advection, dispersion and conduction. The thermoelastic stress has been computed using the analytical solution for simplicity. The pressure was allowed to vary while the discharge was assumed to remain constant along the fracture. A series of numerical simulations were carried out for examining the variation of the fracture aperture and pressure and the results were compared with those obtained without bacterial transport.

The simulation results suggest that temperature and contaminant concentration increase with reduction in initial fracture aperture. The pattern of variation followed by the fracture aperture is nearly the same with and without the influence of bacteria but the magnitude of the fracture aperture is low when subjected to bacterial transport. The reduction in the magnitude of the fracture aperture when subjected to bacterial transport is due to the consumption of contaminants by bacteria as substrate. Consequently, bacterial growth reduces the reservoir efficiency as it affects the fracture permeability significantly. The variation in the fracture aperture resulting from precipitation-dissolution and thermoelastic stresses is significant when the fracture aperture is very low and reduces with increment in fracture aperture. The variation in fracture aperture and pressure is same for both undersaturated and supersaturated fluid entering the fracture due to the influence of bacterial transport at the inlet of the fracture.

## References

- Abdel-Salam, A., Chrysikopolous, C.V., 1994. Analytical solutions for one-dimensional colloid transport in saturated fractures. *Advances in Water Resources* 17, 283–296.
- Abdel-Salam, A., Chrysikopoulos, C.V., 1995. Analysis of a model for contaminant transport in fractured media in the presence of colloids. *Journal of Hydrology* 165, 261–281.
- Arvidson, R.S., Mackenzie, F.T., 1999. The dolomite problem: the control of precipitation kinetics by temperature and saturation state. *American Journal of Science* 299, 257–288.
- Baek, I., Pitt, W.W., 1996. Colloid-facilitated radionuclide transport in fractured porous rock. *Waste Management* 16, 313–325.
- Bodvarsson, G., 1969. On the temperature of water flowing through fractures. *Journal of Geophysical Research* 74, 1987–1992.
- Bourcier, W.L., Lin, M., Nix, G., 2005. Recovery of Minerals and Metals from Geothermal Fluids. SME Annual Meeting. Lawrence Livermore National Laboratory.
- Chrysikopolous, C.V., Abdel-Salam, A., 1997. Modeling colloid transport and deposition in saturated fractures. *Colloids and Surfaces A: Physicochemical and Engineering Aspects* 121, 189–202.
- Cline, J.S., Bodnar, R.J., Rimstidt, D., 1992. Numerical simulation of fluid flow and silica transport and deposition in boiling hydrothermal solutions: applications to epithermal gold deposits. *Journal of Geophysical Research* 97 (B6), 9085–9103.
- Corapcioglu, M.Y., Haridas, A., 1984. Transport and fate of microorganisms in porous media: a theoretical investigation. *Journal of Hydrology* 72, 149–169.
- Corapcioglu, M.Y., Kim, S., 1995. Modeling facilitated contaminant transport by mobile bacteria. *Water Resources Research* 31, 2639–2647.
- Driese, S.G., McKay, L.D., Penfield, C.P., 2001. Lithologic and pedogenic influences on porosity distribution and groundwater flow in fractured sedimentary saporolite: a new application of environmental sedimentology. *Journal of Sedimentology Research* 71 (5), 843–857.
- Fu, L., Milliken, K.L., Sharp Jr., J.M., 1993. Porosity and permeability variations in fractured and lieegang-banded Breathir sandstones (middle Pennsylvanian), eastern Kentucky: diagenetic controls and implications for modeling dual-porosity systems. *Journal of Hydrology* 154, 351–381.
- Ghassemi, A., Suresh Kumar, G., 2007. Changes in fracture aperture and fluid pressure due to thermal stress and silica dissolution/precipitation induced by heat extraction from subsurface rocks. *Geothermics* 36, 115–140.
- Hurtado, R., Mercado, S., Gamino, H., 1989. Brine treatment test for reinjection on cerro prieto geothermal field. *Geothermics* 18, 145–152.
- Ibraki, M., Sudicky, E.A., 1995. Colloid-facilitated contaminant transport in discretely fractured porous media-I numerical formulation and sensitivity analysis. *Water Resources Research* 31, 2945–2960.
- Kim, S.B., 2005. Contaminant transport and biodegradation in saturated porous media: model development and simulation. *Hydrological Processes* 19, 4069–4079.
- Kim, S.B., 2006. Numerical analysis of bacteria transport in saturated porous media. *Hydrological Processes* 20, 1177–1186.
- Kim, S., Corapcioglu, M.Y., 1996. A kinetic approach to modeling mobile bacteria-facilitated groundwater contaminant transport. *Water Resources Research* 32, 321–331.
- Lowell, R.P., Van Cappellen, P., Germanovich, L.N., 1993. Silica precipitation in fractures and the evolution of permeability in hydrothermal upflow zones. *Science* 260, 192–194.
- Malate, R.C.M., O'Sullivan, M.J., 1992. Mathematical modeling of non-isothermal silica transport and deposition in a porous medium. *Geothermics* 21, 519–544.
- McLin, K.S., Moore, J.N., Hulen, J., Bowman, J.R., Berard, B., 2006. Mineral characterization of scale deposits in injection wells; Coso and Salton Sea geothermal fields, CA. In: *Proceedings of Thirty First Workshop on Geothermal Reservoir Engineering*. Stanford University, California.
- Natarajan, N., Suresh Kumar, G., 2010a. Effect of thermo and poroelasticity on the evolution of fluid permeability in a coupled fracture-skin-matrix system. In: *Proceedings of the Ninth International Conference on Hydro-science and Engineering*. August 2–5.
- Natarajan, N., Suresh Kumar, G., 2010b. Radionuclide and colloid co-transport in a coupled fracture-skin-matrix system. *Colloids and Surfaces A: Physicochemical and Engineering Aspects* 370, 49–57.
- Natarajan, N., Suresh Kumar, G., 2011a. Numerical modeling and spatial moment analysis of thermal fronts in a coupled fracture-skin-matrix system. *Geotechnical and Geological Engineering* 29, 477–491.
- Natarajan, N., Suresh Kumar, G., 2011b. Numerical modelling of bacteria facilitated contaminant transport in fractured porous media. *Colloids and Surfaces A: Physicochemical and Engineering Aspects* 387, 104–112.
- O'Brien, G.S., Bean, C.J., McDermott, F., 2003. Numerical investigations of passive and reactive flow through generic single fractures with heterogeneous permeability. *Earth and Planetary Science Letters* 213, 271–284.
- Polak, A., Grader, A.S., Wallach, R., Nativ, R., 2003. Chemical diffusion between a fracture and the surrounding matrix, measurement by computed tomography and modeling. *Water Resources Research* 39 (4), 1106.
- Potapov, V.V., Karpov, G.A., Podverbnyi, V.M., 2002. Removal of silica from geothermal brine. *Theoretical Foundations of Chemical Engineering* 36 (6), 589–595.
- Rimstidt, J.D., Barnes, H.L., 1980. The kinetics of silica-water reactions. *Geochimica et Cosmochimica Acta* 44, 1683–1699.
- Robinson, B.A., 1982. Quartz dissolution and silica deposition in hot dry rock geothermal systems. M.S. thesis, MIT.
- Robinson, N.I., Sharp, J.M., Kreisel, I., 1998. Contaminant transport in sets of parallel finite fractures with fracture skins. *Journal of Contaminant Hydrology* 31, 83–109.
- Robinson, B.A., Pendergrass, J., 1989. A combined heat transfer and quartz dissolution/deposition model for a hot dry rock geothermal reservoir. In: *Proceedings of the 14th Stanford Geothermal Workshop*. Stanford University, pp. 207–212.
- Robinson, N.I., Sharp Jr., J.M., 1997. Analytical Solution for Contaminant Transport in a Finite Set of Parallel Fractures with Matrix Diffusion. C.S.I.R.O. Mathematical and Information Sciences, Report CMIS-C23, 26 pp.
- Sand, W., 2003. Microbial life in geothermal waters. *Geothermics* 32, 655–667.
- Satman, A., Ugur, Z., Onur, M., 1999. The effect of calcite deposition on geothermal well inflow performance. *Geothermics* 4 (1), 425–444.
- Sen, T.K., Das, D., Khilar, K.C., Suraishkumar, G.K., 2005. Bacterial transport in porous media: new aspects of the mathematical model. *Colloids and Surfaces A* 260, 52–62.
- Sharp, J.M., 1993. Fractured aquifers/reservoirs: approaches, problems, and opportunities. In: Banks, D., Banks, S. (Eds.), *Hydrogeology of Hard Rocks*, Memoires of the 24 th Cong. International Assoc. Hydrogeologists. Oslo Norway 24 Part 1, pp. 23–28.
- Steeffel, C.I., Lichtner, P.C., 1998. Multicomponent reactive transport in discrete fractures. I. Controls on reaction front geometry. *Journal of Hydrology* 209, 186–199.
- Suresh Kumar, G., Ghassemi, A., 2005. Numerical modeling of non-isothermal quartz dissolution in a coupled fracture–matrix system. *Geothermics* 34, 411–439.
- Taron, J., Elsworth, D., 2009. Thermal–hydrologic–mechanical–chemical processes in the evolution of engineered geothermal reservoirs. *International Journal of Rock Mechanics and Mining Sciences* 46, 855–864.
- Taron, J., Elsworth, D., Min, K., 2009. Numerical simulation of thermal-hydrologic-mechanical-chemical processes in deformable, fractured porous media. *International Journal of Rock Mechanics and Mining Sciences* 46, 842–854.
- Yun, Z., 1986. Thermophilic microorganisms in the hot springs of Tengchong geothermal area, West Yunnan, China. *Geothermics* 15, 347–358.